



# Potential of Local Natural Bentonite Impregnated with N-TiO<sub>2</sub> to Degrade Methylene Blue Using Photocatalytic Process

TECHNICAL ARTICLE

u[ubiquity press

ADHI SETIAWAN

VIRA FADILAH QUR'ANI

TARIKH AZIS RAMADANI

MOCHAMAD LUQMAN ASHARI

DENNY DERMAWAN

ADITYA PRANA ISWARA

\*Author affiliations can be found in the back matter of this article

## ABSTRACT

The wastewater from the textile industry generally contains toxic chemicals methylene blue that are difficult to degrade by the environment. This study aims to develop a high-performance natural photocatalyst from Bentonite impregnated by N-TiO<sub>2</sub> with a high photodegradation rate for methylene blue removal under UV and visible light. Characterization of the material was conducted using SEM-EDX, XRD, and FTIR. The EDX results showed that elemental N had been detected in N-TiO<sub>2</sub> and N-TiO<sub>2</sub>/activated bentonite. The FTIR spectra showed that the absorption peak of N-TiO<sub>2</sub>/activated bentonite is similar to that of activated bentonite and N-TiO<sub>2</sub>. The N-TiO<sub>2</sub>/activated bentonite diffractogram showed the peaks of quartz and montmorillonite minerals. The N-TiO<sub>2</sub>/activated bentonite photocatalyst resulted in a decrease in the bandgap energy of 3.06 eV. The decline in band gap energy on N-TiO<sub>2</sub>/activated bentonite is higher than the decrease in band gap energy for N-TiO<sub>2</sub>. The optimum pH condition for the photocatalyst process in removing methylene blue occurs at pH 5. The maximum removal efficiency of methylene blue occurs when the ratio of N: Ti is 1:1 with an irradiation time under UV and visible lights of 120 minutes of 99.23% and 87.20%, respectively. This study showed that the composite catalyst N-TiO<sub>2</sub>/bentonite under UV and visible light irradiation conditions has higher removal efficiencies on lower dosages (2.5–10 times lower in dosage), higher initial methylene blue concentration (1.25–2.5 times higher in concentration), and shorter reaction (1.5–3 times shorter in irradiation time) than composite catalysts from previous studies' results. Furthermore, the product can enhance the value of local natural bentonite and increase local people's income and welfare.

## CORRESPONDING AUTHOR: Aditya Prana Iswara

Department of Disaster Management, Postgraduate School, Universitas Airlangga, Surabaya, Indonesia  
aditya.prana@pasca.unair.ac.id

## KEYWORDS:

Activated bentonite; Methylene blue; N-TiO<sub>2</sub>; Photocatalytic; UV and visible light; Langmuir-Hinshelwood kinetic

## TO CITE THIS ARTICLE:

Setiawan, A, Qur'ani, VF, Ramadani, TA, Ashari, ML, Dermawan, D and Iswara, AP. 2024. Potential of Local Natural Bentonite Impregnated with N-TiO<sub>2</sub> to Degrade Methylene Blue Using Photocatalytic Process. *Future Cities and Environment*, 10(1): 14, 1–17. DOI: <https://doi.org/10.5334/fce.220>

## 1. INTRODUCTION

One industry that consumes a disproportionately large amount of water is the textile industry (Dilaver et al., 2018). Wastewater from the textile industry typically contains hazardous compounds that are difficult for the environment to break down (Fayoud et al., 2016). Acids, starches, hydrogen peroxide, alkalis, and dyes are frequently used chemicals. Methylene blue is a synthetic dye frequently used in textile dyeing production (Benhouria et al., 2015). Wastewater will absorb about 15% of the synthetic dyes used in the textile sector (Tichapondwa et al., 2020). Low molecular weight and aromatic and amine groups in the structure of methylene blue make it poisonous, carcinogenic, and challenging to break down in the environment (Imron et al., 2019).

Diverse techniques, including coagulation-flocculation, adsorption, and membrane filtering, have been developed to remove color content in wastewater, such as methylene blue (Dermawan et al., 2022; Echabbi et al., 2019). Although this technique effectively removes colors from wastewater, it has a drawback in that contaminants are only moved from one phase to another without being degraded (Gong et al., 2015). Using conventional methods still necessitates additional procedures for treating the sludge or trash produced, which raises the cost of operation (Daghrir et al., 2013). Aerobic and anaerobic procedures used to treat wastewater containing synthetic dyes have low dye removal efficiencies, leaving wastewater still colored and visible in the environment (Pan et al., 2017).

The Advanced Oxidation Process (AOP), which can reduce dyes in wastewater, includes photocatalysis. Strong oxidizing agents, hydroxyl radicals created by the AOP process, demineralize organic substances to produce water, carbon dioxide, and mineral acids to reduce waste products' production (Sanchez et al., 2010; Setiawan et al., 2023). Photocatalytic techniques are a novel and successful wastewater treatment method for breaking down organic contaminants into carbon dioxide and water utilizing light energy (Raza et al., 2020). When used commercially, photocatalyst can be more profitable than conventional wastewater treatment since it is more sustainable and energy-efficient (W. Wang et al., 2020).

Great abundance, low toxicity, high stability, and outstanding photocatalytic activity are just a few benefits of the  $\text{TiO}_2$  photocatalytic process (Zhang et al., 2015). The strong oxidation properties of  $\text{TiO}_2$  make it an ideal semiconductor type that can boost the mineralization efficiency of organic contaminants that are difficult for the environment to degrade (Anwer & Park, 2019). One drawback of employing  $\text{TiO}_2$  is the need for high-energy UV radiation during photocatalyst activation (Chien et al., 2015). Since the band gap of pure  $\text{TiO}_2$  is relatively high (3.2 eV for anatase), photocatalytic activity can only occur when exposed to UV radiation (Sinhamahapatra et al.,

2015). Reduce the energy band gap by doping  $\text{TiO}_2$  with specific compounds (Gil et al., 2017). Metal elements (Ag, Au, Cu, and Ni) (Hou et al., 2018), as well as non-metallic elements (B, S, F, and C) (Yeoh & Chan, 2017), have been used as doping materials for  $\text{TiO}_2$  in several investigations. Metal doping can lower carrier mobility by creating an extremely confined d state in the band gap and creating electron-hole recombination sites, drastically reducing the photocatalytic performance (Hoang et al., 2012). Due to the similarities between the elements O and N in terms of ionic radius, electronegative properties, and polarization, the synthesis of N-doped  $\text{TiO}_2$  has been the research focus (F. Wang et al., 2021).

The rate of photocatalytic reduction is relatively low since the adsorption power of photocatalyst materials is often lower than that of adsorbent materials (Matos et al., 1998). According to Djellabi et al. (Djellabi et al., 2015), forming a hydrophobic layer by  $\text{TiO}_2$  particles dispersed in montmorillonite minerals can enhance the capacity of organic dye pollutants to photodegrade in wastewater. Zeolite, kaolin, sepiolite, and bentonite are among the clay minerals that may undergo  $\text{TiO}_2$  dispersion. These minerals can create  $\text{TiO}_2$  composites because they are thermally stable, have larger pores, and make separation easier (Rossetto et al., 2010). One kind of clay mineral that is frequently employed as an adsorbent is bentonite. Bentonite can be used because of its small colloidal particle size and high ionic surface area. Bentonite possesses adsorption properties to increase the photocatalytic activity of  $\text{TiO}_2$  (Setiawan et al., 2024). Bentonite material is a cheap and economical alternative that should be considered a supporting material for photocatalysts. Bentonite is abundantly available in the form of Na-montmorillonite or Ca-montmorillonite in various countries, including the United States, Russia, Brazil, Africa, and Asia-Pacific. East Java is one of the largest natural bentonite-producing provinces in Indonesia. Natural bentonite mines in East Java are scattered in several cities, including Blitar, Trenggalek, Ponorogo, and Pacitan, with production reaching 500 million tonnes. Generally, bentonite in Indonesia is often applied to several industries, such as cooking oil, oil drilling, and cosmetics (Koswojo et al., 2010). Using natural bentonite as a supporting material in wastewater treatment is still limited. Several studies have developed bentonite as a wastewater treatment material. The synthesis of organo-bentonite to adsorb ampicillin from wastewater (Rahardjo et al., 2011) and the adsorption of methylene blue using alginate-encapsulated bentonite (Ravi & Pandey, 2019). Then the adsorption of rhodamin B and acid red using organo-bentonite (Huang et al., 2017), adsorption of Cu(II) and Ni(II) in wastewater using bentonite/graphene oxide (Chang et al., 2020), and photodegradation of methylene blue using ZnO-modified bentonite (Sasikala et al., 2019).

However, our research data shows that using natural bentonite from Indonesia as a supporting material in

the photocatalytic process is still limited. This study aims to synthesize modified N-TiO<sub>2</sub> using natural bentonite as a photocatalytic material to reduce wastewater's methylene blue content. Methylene blue was selected to indicate photocatalyst performance as a cationic dye with numerous medical, textile, and printing applications. This study examined the impact of pH factors, the N-to-Ti ratio, and contact time on methylene blue's degradation. Then the photocatalyst process for removing methylene blue used visible and UV-A light sources. Methylene concentration reduction data obtained from the photocatalytic process were further analyzed using a kinetic model. Characterization of the N-TiO<sub>2</sub>/bentonite catalyst obtained using Scanning Electron Microscope-Energy Dispersive X-ray (SEM-EDX), X-ray diffraction (XRD), Fourier transform infrared spectroscopy (FTIR), and UV-visible diffuse reflectance spectroscopy (DRS).

## 2. MATERIAL AND METHODS

The main material in this study is the local bentonite acquired from Blitar Regency, East Java. By introducing TiO<sub>2</sub> to the local bentonite, an increase in adsorption capacity can be achieved. Figure 1 presents the experimental procedure conducted in this study.

### 2.1. PREPARATION OF N-TiO<sub>2</sub>

The synthesis process of N-doped TiO<sub>2</sub> was carried out by referring to experiments that had been carried out

by Marques (Marques et al., 2019) and Bakre (Bakre et al., 2020) with several modifications. Synthesis of N-TiO<sub>2</sub> using urea powder and TiO<sub>2</sub> mixed with mole ratios of 1:1, 2:1, and 3:1. The mass of each component of the mixture was then agitated until it was homogenous. It was then dissolved into deionized water at a 1:2 mass-to-volume ratio. The combination was then put through a 30-minute sonication process (using an Ultrasonic Cleaner POWER SONIC 405) (Chien et al., 2015). For three hours, the suspension was evaporated in an oven set at 105°C. N-TiO<sub>2</sub> samples were calcined in a furnace (Thermolyne) at 500°C for two hours, and the process was finished by flattening the sample in a mortar until it became powder.

### 2.2. PREPARATION OF ACTIVATED BENTONITE

The bentonite used in this study was obtained from a bentonite mining site in Blitar Regency, East Java Province, Indonesia. The bentonite obtained was then cleaned and dried at 105°C in the oven (Binder ED 53) for 24 hours. Chemical activation of bentonite was accomplished with an HCl solution (Merck, USA). With a few adjustments, the bentonite activation procedure was based on the research (Toor et al., 2015). A 1:2 mass ratio of natural bentonite to solution volume was used when submerged in a 2 M HCl solution.

Additionally, stirring was done for two hours at 100 rpm using a magnetic stirrer (Thermo Scientific). Aquabidest was used to rinse the activated bentonite. A mortar and 100 mesh sieve were used for crushing and sifting activated bentonite.

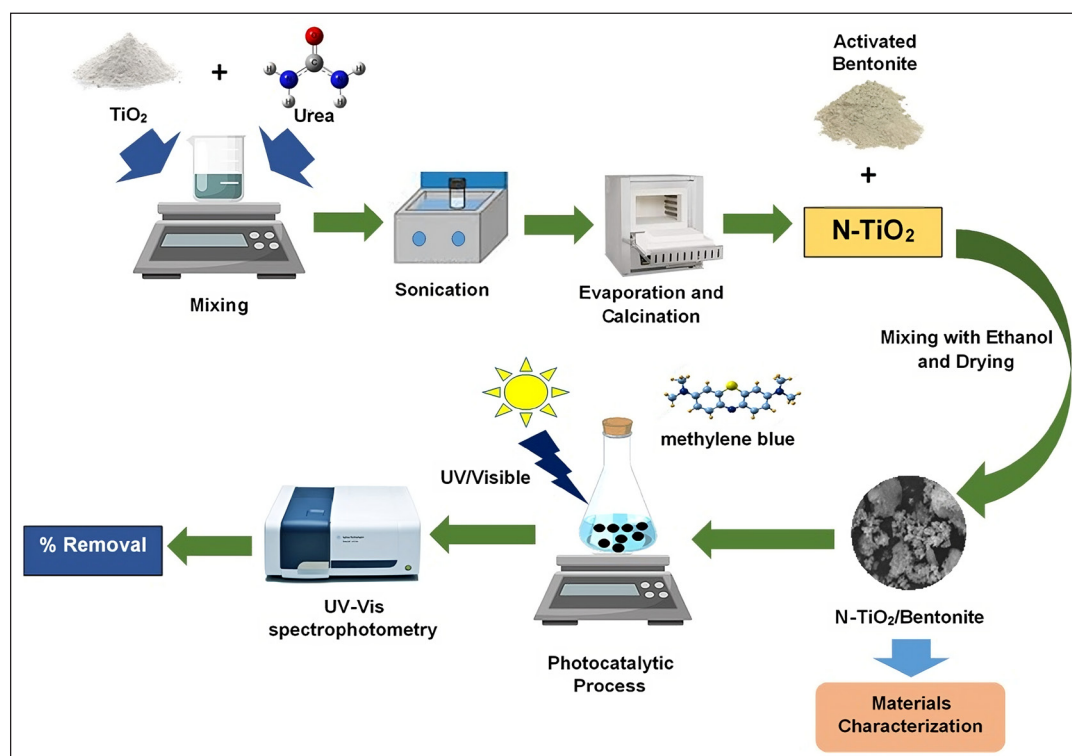


**Figure 1** Experimental procedure for the synthesis of N-TiO<sub>2</sub>/activated bentonite to reduce methylene blue dye.

### 2.3. PREPARATION OF N-TiO<sub>2</sub> IMPREGNATION WITH ACTIVATED BENTONITE

The N-TiO<sub>2</sub>/Activated Bentonite impregnation procedure was based on studies by Gar et al. (Gar Alalm et al., 2016). In a 100 mL beaker, first, combine 0.4 grams of N-TiO<sub>2</sub> and 1 gram of activated bentonite. Added 6 mL of 96% ethanol, then homogenized the mixture for 5 hours using a magnetic stirrer. N-TiO<sub>2</sub>/activated bentonite was dried in a 200°C oven for 5 hours. N-TiO<sub>2</sub>/activated bentonite was mashed in a mortar and sieved through a 100-mesh sieve.

### 2.4. PREPARATION OF METHYLENE BLUE SOLUTION

All the chemicals used in this research were of the analytical reagent grade. Methylene blue (MB) was purchased from Merck, USA. 1.0 g MB was dissolved in 100 ml of distilled water to make a stock solution containing 100 mg/L of MB. Diluting the stock solution yielded MB solutions of a concentration of 25 mg/L for photocatalytic experiments. A single beam UV-VIS spectrophotometer (Agilent Cary 60, USA) with a λ<sub>max</sub> of 655 nm was used to measure MB concentration at each trail of the photocatalytic process. Each pH solution was altered using either 0.1 M sodium hydroxide or 0.1 M hydrochloric acids and measured by a pH meter (SP-2300, SUNTEX, Taiwan).

### 2.5. PHOTOCATALYTIC PROCESS

The experimental procedure of the photocatalytic reaction involves mixing 0.02 grams of N-TiO<sub>2</sub>/activated bentonite with 100 mL of 25 mg/L methylene blue solution. Methylene blue solution and catalyst are contacted for 30 minutes to reach adsorption and desorption equilibrium before irradiation. In the first stage, a photocatalytic process was carried out with pH 5, 7, 9, and 11 variations to obtain the optimum pH. Furthermore, the optimum pH used in the photocatalytic process was run at 100 rpm for 15, 30, 45, 60, 75, 90, and 120 minutes with UV-A (8-watt) and visible light (LED 8-watt) irradiation. 2,500 rpm centrifuging for 10 minutes to separate the adsorbent from the filtrate. Use the injection to remove the filtrate from the tube carefully. The next step was to use a UV-Vis spectrophotometer with a wavelength of 655 nm to measure the final concentration of methylene blue. The equation was used to determine methylene blue's ability to degrade as Eq. (1):

$$\% \text{Removal} = \frac{C_0 - C_t}{C_0} \times 100\% \quad (1)$$

C<sub>0</sub> and C<sub>t</sub> were the amounts of methylene blue (mg/L) before and after the photocatalyst process.

Quality Assurance (QA)/Quality Control (QC) for methylene blue concentration testing using a spectrophotometer is carried out with several applications including the use of blank samples, a methylene blue calibration curve with a correlation coefficient of 0.997 (correlation coefficient in Indonesian

National Standard (SNI) > 0.995), sample duplication with a relative percent difference (RPD) value of <10%, use of reagents with pro-analysis quality, and calibration of measuring instruments.

The kinetics of the methylene blue degradation reaction were examined using the data on methylene blue concentrations collected following the photocatalyst process. The Langmuir-Hinshelwood kinetic model used in the photocatalyst reaction kinetics model can be expressed as equation (2) (Jawad et al., 2016; Kuo et al., 2011):

$$\ln\left(\frac{C_0}{C_t}\right) = k_{app}t \quad (2)$$

Where k<sub>app</sub> is the pseudo-first-order rate constant (min<sup>-1</sup>), and t is the reaction time (min). K<sub>app</sub> constant is the slope determined by linear regression of ln(C<sub>0</sub>/C<sub>t</sub>) vs t.

### 2.6. COMPOSITE CHARACTERIZATION

The phases of N-TiO<sub>2</sub>-activated bentonite and N-TiO<sub>2</sub>/activated bentonite were examined using XRD (X'pert PRO PANalytical). Cu ka monochromator radiation (λ = 1.5405) at 30 kV and 30 mA, 2 = 5–60°, was used in the XRD analysis. The functional groups of N-TiO<sub>2</sub>-activated bentonite and N-TiO<sub>2</sub>/activated bentonite were examined using the Fourier transform-infrared (FTIR) spectrum in the 400–4000 cm<sup>-1</sup>. The KBr pellet technique was used to conduct the study using a Fourier transform infrared spectrometer (Thermo Scientific Nicolet iS10). Scanning Electron Microscope-Energy Dispersive X-Ray (SEM-EDX) Inspect S50 operating at 20 kV was used to examine the surface morphology of N-TiO<sub>2</sub>, activated bentonite, and N-TiO<sub>2</sub>/activated bentonite. Bandgap energy measurement of TiO<sub>2</sub>, N-TiO<sub>2</sub>, and N-TiO<sub>2</sub>/activated bentonite was carried out using UV-Vis Diffuse Reflectance Spectroscopy (Analytik Jena, Specord 200 Plus). Between 300 to 800 nm, the band gap energy analysis was compared to the % reflectance. Equation 3 was used to analyze UV-Vis DRS data using the Kubelka-Munk function (Calisir et al., 2020) with a Tauc-plots:

$$(F(R).hv)^x = \left\{ \frac{(1-R)^2}{2R} . hv \right\}^{0.5} \quad (3)$$

The sample band gap energy is determined from the spectra by plotting between (F(R) hv)<sup>0.5</sup> as the Y axis and the photon energy as the X axis. The x value in equation (3) is taken as 0.5 because TiO<sub>2</sub> has an indirect band gap. The band gap is determined from the vertical line drawn until it intersects the x-axis on the graph plot (F(R)hv)<sup>0.5</sup> vs hv.

## 3. RESULTS AND DISCUSSIONS

### 3.1. CHARACTERIZATION OF THE COMPOSITE CATALYST

The provided SEM image characterized the catalyst material employed in this investigation. Figure 2 shows

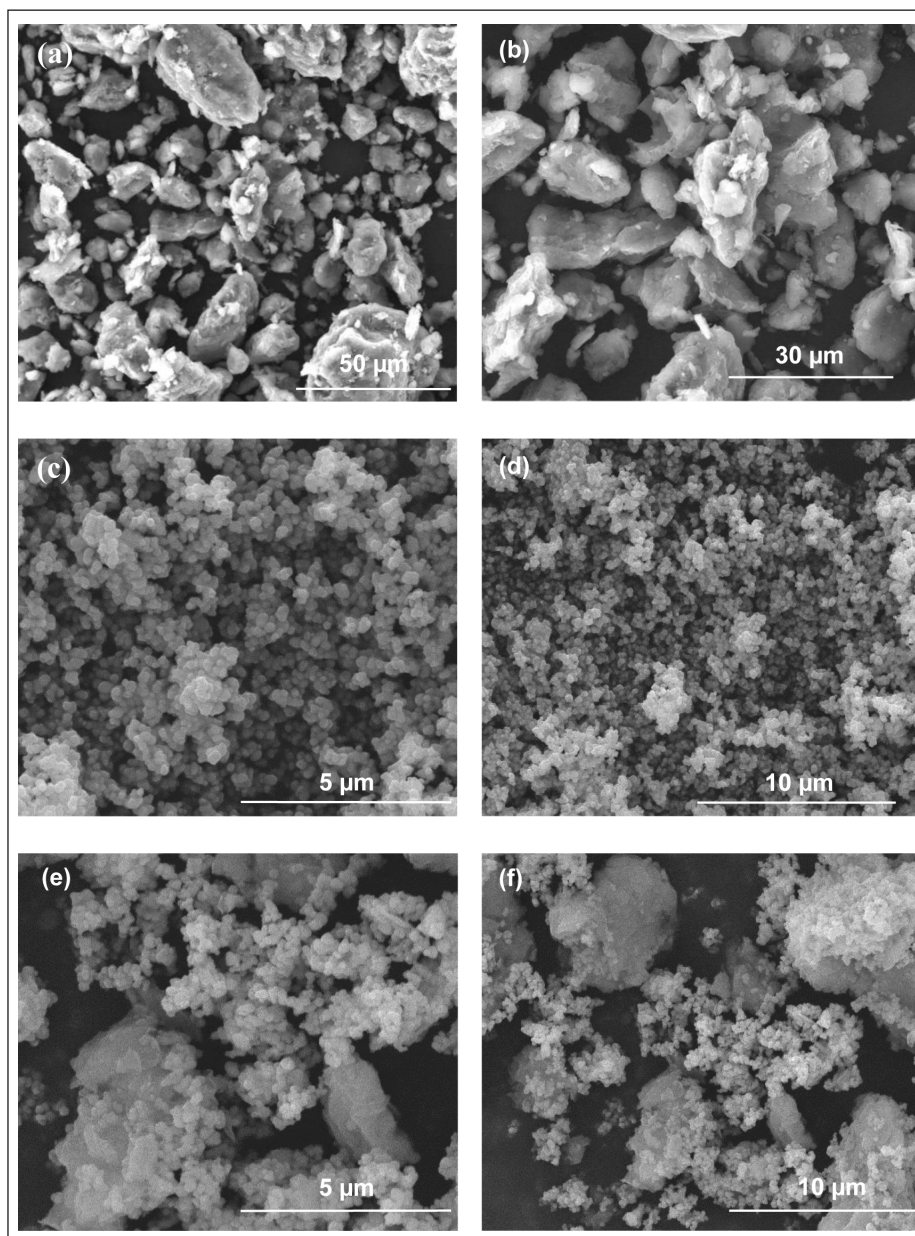


**Figure 2** SEM of Activated Bentonite (a,b), N-TiO<sub>2</sub> (N:Ti = 1:1) (c, d), and N-TiO<sub>2</sub>/Activated Bentonite (with N:Ti = 1:1) (e, f).

the results of the SEM study of activated bentonite (a) and (b), N-TiO<sub>2</sub> (c) and (d), and N-TiO<sub>2</sub>/activated bentonite (e) and (f). Particle aggregates predominate on the surface of activated bentonite, big, and smooth in appearance. The figure shows a smooth surface caused by mineral acid (HCl) activation, which removes impurity components such as tar and calcium salts that cover the bentonite pores. The activation process modifies the bentonite surface, increasing its contaminant adsorption ability (Chen et al., 2013). In their respective studies, according to Chen et al. (Chen et al., 2013) and Natsir et al. (Natsir et al., 2021), activated bentonite was also created with a similar surface morphology. Spherical and lumpy features predominate on the surface of N-TiO<sub>2</sub>. N-TiO<sub>2</sub> with a 0.27 μm average size. The surface morphology of activated N-TiO<sub>2</sub>/bentonite comprised tiny aggregates with an average size of 1.08 μm and an

uneven structure. Small aggregates were particle pieces and lumps of N-TiO<sub>2</sub> crystallites that formed due to the hydrolysis of Ti on the surface (Chen et al., 2013). Particle size and standard deviation are presented in Table 1.

The findings of the EDX test on activated bentonite, N-TiO<sub>2</sub>, and N-TiO<sub>2</sub>/activated bentonite were employed for quantitative analysis. Furthermore, Table 2 displays the results of an EDX investigation on activated bentonite, N-TiO<sub>2</sub>, and N-TiO<sub>2</sub>/activated bentonite. The primary components of montmorillonite are Si, O, and Al (Hrachová et al., 2007). The EDX results showed that elemental N had been detected in N-TiO<sub>2</sub> and N-TiO<sub>2</sub>/activated bentonite, indicating that the N impregnation process was successfully carried out. Then this is consistent with the EDX analysis results of activated bentonite, which found the highest concentrations of Si, O, and Al, respectively, 33.45%, 38.25%, and 18.71%.

SAMPLE	PARTICLE SIZE ( $\mu\text{m}$ )	STANDARD DEVIATION
Activated Bentonite	9.57	2.13
N-TiO <sub>2</sub> (N:Ti = 1:1)	0.27	0.05
N-TiO <sub>2</sub> /Activated Bentonite (N:Ti = 1:1)	1.08	0.38

**Table 1** Particle Size and Standart Deviation.

ELEMENT	ACTIVATED BENTONITE (%)	N-TiO <sub>2</sub> (N:Ti = 1:1) (%)	N-TiO <sub>2</sub> /ACTIVATED BENTONITE (N:Ti = 1:1) (%)
O	38.25	36.78	44.66
Na	1.37	0	1.02
Mg	2.18	0	1.03
Al	18.71	0	7.47
Si	33.45	0	12.48
Fe	6.04	0	3.46
N	0	3.93	1.12
Ti	0	59.29	28.76

**Table 2** Test Results of EDX.

Si and Al content in N-TiO<sub>2</sub>/activated bentonite were lower (12.48 and 7.47%) than in activated bentonite. Natsir et al. (Natsir et al., 2021) revealed that Si and Al's elements were present in amounts of 11.35% and 7.53%, respectively. The presence of impregnated Ti content on the surface of activated bentonite may cause a decrease in Si and Al composition in N-TiO<sub>2</sub>/activated bentonite.

On activated bentonite, N-TiO<sub>2</sub>, and N-TiO<sub>2</sub>/activated bentonite, FTIR analysis in the 4000–500 cm<sup>-1</sup> range was performed. The spectrum plots for activated bentonite, N-TiO<sub>2</sub>, and N-TiO<sub>2</sub>/activated bentonite from the FTIR analysis are shown in Figure 3.

Compared to N-TiO<sub>2</sub>/activated bentonite, the FTIR spectra of activated bentonite displayed absorption bands at 3621.07 and 3383.03 and 3603.13 and 3352.22 cm<sup>-1</sup>, respectively. The Al-OH, Si-OH, and interlayer water molecules' stretching vibration correlates with the absorption band. When TiO<sub>2</sub> is impregnated with activated bentonite, the absorption band moves to a lower wave number caused by the presence of hydrated pure cations and dehydroxylated H<sub>2</sub>O in TiO<sub>2</sub> (Hadj Bachir et al., 2020). The Ti-O stretching vibration of the TiO<sub>2</sub> phase, Ti-O-Ti, and Ti-O-Si bonds can be seen in the absorption bands between 500 and 1000 cm<sup>-1</sup>.

Additionally, the impregnation procedure results in the anatase group being. The impregnation procedure results in the anatase group being tightly chemically bonded to the silicate (Li et al., 2002). N-TiO<sub>2</sub>/activated bentonite lacks several absorption areas in activated bentonite, and the impregnation process with TiO<sub>2</sub> may cause their absence. As a result, the anions in the titanium layer replace those in the montmorillonite layer (Djellabi et al., 2015). The

absorption peak of N-TiO<sub>2</sub>/activated bentonite is similar to that of activated bentonite and N-TiO<sub>2</sub>, demonstrating that no chemical reactions occur during the impregnation process (Javanbakht & Mohammadian, 2021).

The mineral content and crystal phase of activated bentonite, N-TiO<sub>2</sub>, and N-TiO<sub>2</sub>/activated bentonite were examined using the peak pattern of the XRD test findings. Figure 4 compares the peak patterns obtained from the XRD analyses of activated bentonite, N-TiO<sub>2</sub>, and N-TiO<sub>2</sub>/activated bentonite. The peak pattern of the XRD test findings was used to determine the mineral composition and crystal phase of activated bentonite, N-TiO<sub>2</sub>, and N-TiO<sub>2</sub>/activated bentonite. Figure 3 compares the peak patterns from the XRD analyses of N-TiO<sub>2</sub>, activated bentonite, and N-TiO<sub>2</sub>/activated bentonite.

The N-TiO<sub>2</sub> diffraction pattern shows peaks with the maximum intensities at positions 2 $\theta$  are 25,215°, 36,847°, 37,691°, 38,474°, 47,955°, 53,833°, and 55,007°. Based on JCPDS No. 021-1272, which indicates that the anatase phase dominates the peak patterns of N-TiO<sub>2</sub>. The features of anatase were discovered in the diffraction peaks of 2 $\theta$  = 25°, 38°, 48°, 54°, and 55°, according to research done by Ma et al. (Ma et al., 2021). The N peak was not visible in the XRD analysis results, which might result from the high purity of TiO<sub>2</sub>, which prevented the identification of the N peak (Calisir et al., 2020). According to Xu et al. (Xu et al., 2019), the lack of an N peak in the XRD pattern suggests no N element aggregation because the N doping can be distributed uniformly throughout the TiO<sub>2</sub> lattice structure without affecting the crystal phase structure of TiO<sub>2</sub>.

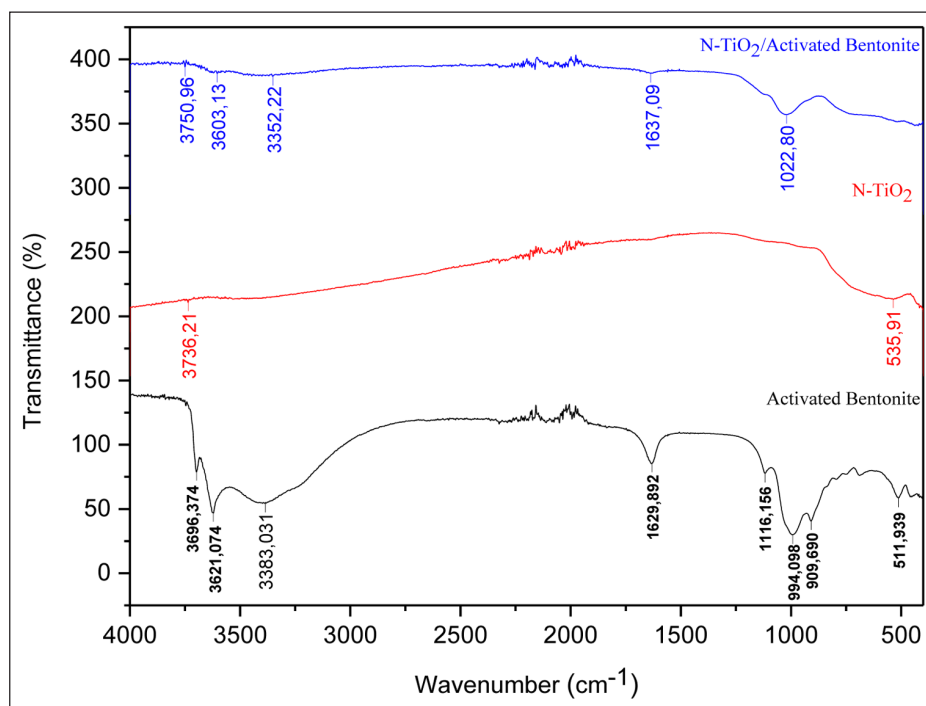


**Figure 3** FTIR Spectra of Activated Bentonite, N-TiO<sub>2</sub> (N:Ti = 1:1) and N-TiO<sub>2</sub>/Activated Bentonite (with N:Ti = 1:1).

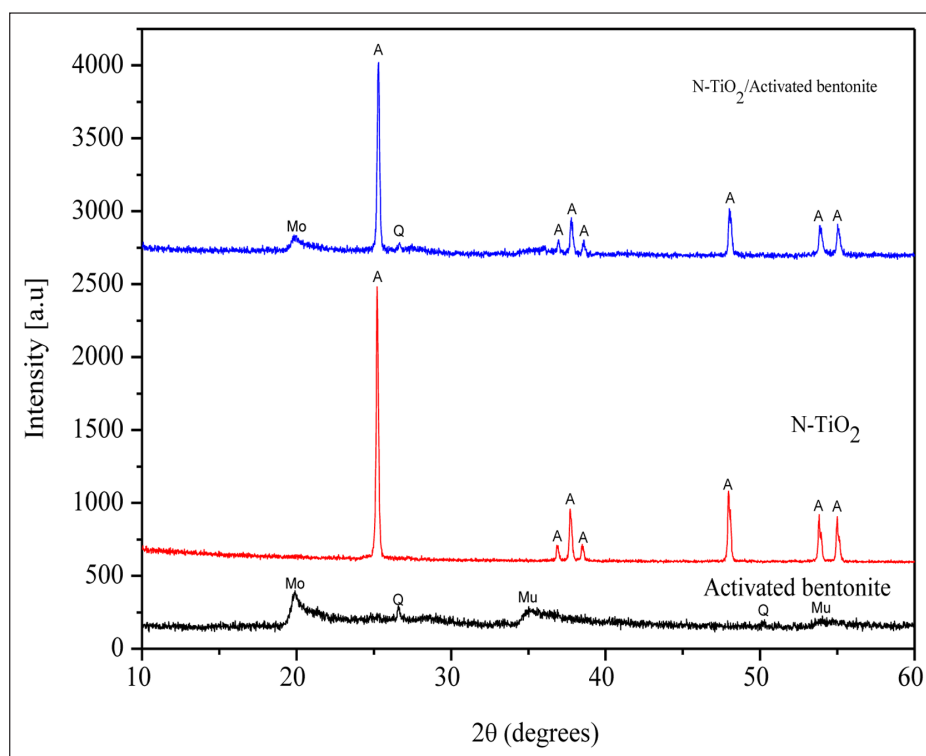


**Figure 4** XRD of Activated Bentonite, N-TiO<sub>2</sub> (N:Ti = 1:1) and N-TiO<sub>2</sub>/Activated Bentonite (with N:Ti = 1:1). (A = anatase, Mu = montmorillonite, and Q = quartz).

The N-TiO<sub>2</sub>/activated bentonite diffractogram showed the peaks of quartz and montmorillonite minerals. SiO<sub>2</sub> and montmorillonite comprise the fundamental components of bentonite, which showed no structural change during the N-TiO<sub>2</sub>/activated bentonite impregnation procedure. The N-TiO<sub>2</sub>/activated bentonite diffractogram showed a reduction in intensity and numerous peak intensities of activated bentonite diffraction, which could happen if

titanium ions replace the calcium hydrate in bentonite (F. Wang et al., 2021). The number of anatase TiO<sub>2</sub> peaks formed was also revealed by studying the activated N-TiO<sub>2</sub>/bentonite diffractogram.

In order to determine the band gap energies of TiO<sub>2</sub>, N-TiO<sub>2</sub>, and N-TiO<sub>2</sub>/activated bentonite, the Kubelka-Munk equation analysis on the DRS spectra data was performed. Figure 5 displays the Tauc plot of the Kubelka-

Munk equation, and Table 3 summarizes the band gap energy values that were determined.

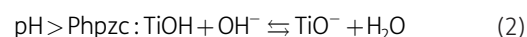
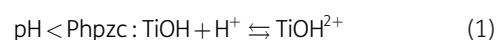
N-TiO<sub>2</sub> and N-TiO<sub>2</sub>/activated bentonite's band gap energy moved to lower energy than TiO<sub>2</sub>'s. The introduction of N atoms into the TiO<sub>2</sub> crystal lattice causes the band gap energy to narrow, resulting in a lower band gap energy. Because the ionic radii of nitrogen and oxygen are similar, nitrogen was chosen as the dopant on TiO<sub>2</sub> (Ansari et al., 2016). The N-TiO<sub>2</sub>/activated bentonite photocatalyst resulted in a decrease in the bandgap energy of 3.06 eV. The decrease in band gap energy on N-TiO<sub>2</sub>/activated bentonite is higher than the decrease in band gap energy for N-TiO<sub>2</sub>. Including a buffer material may lower a sample's band gap energy. The surface area of the photocatalyst material can be increased by dispersing TiO<sub>2</sub> on the activated bentonite surface with the help of a buffer substance. According to Martin et al. (Martins et al., 2017), the TiO<sub>2</sub> photocatalyst's band gap energy could be lowered from 3.07 eV to 3.04 eV by adding activated carbon.

### 3.2. EFFECT OF PH ON METHYLENE BLUE REMOVAL

pH is one critical variable affecting how well the methylene blue dye is removed. At pH 5, 7, 9, and 11, respectively, the effective pH of photocatalysis was measured under four distinct situations. Methylene blue's removal capacity was highest at pH 5 and lowest at pH 9, but it got better at pH 11 as well. Figure 5 shows the results of a test to determine how the pH of the methylene blue dye solution affected the ability of the activated N-TiO<sub>2</sub>/

activated bentonite composite photocatalyst to reduce the dye.

At pH 5, methylene blue was most easily removed, and pH 9 was the least easily removed. However, at pH 11, methylene blue was more easily removed. Figure 6 displays the findings of an experiment testing the impact of the pH of the methylene blue dye solution on the efficiency of the N-TiO<sub>2</sub>/activated bentonite composite photocatalyst in reducing methylene blue dye. At pH<sub>pzc</sub> circumstances, the TiO<sub>2</sub> photocatalyst tends to clump together. Konstantinou et al. (Konstantinou & Albanis, 2004) claimed that TiO<sub>2</sub> clumping reduces the surface area available for dye adsorption and photon absorption, lowering the dyestuff's capacity for reduction. The dye's capacity to reduce has diminished. Reactions (1) and (2) (Konstantinou & Albanis, 2004) show the reaction pathway under pH<sub>pzc</sub> conditions.



Photocatalysts often have surface charges based on pH. Methylene blue dye removal efficiency increased with decreasing pH. Under acidic pH conditions, strong dye adsorption on TiO<sub>2</sub> particles is caused by the electrostatic attraction of positively charged TiO<sub>2</sub> and the dye. Alkaline pH causes the dye molecules to be negatively charged, so their adsorption ability will be influenced by increasing the density of TiO<sup>-</sup> groups on the surface. Therefore, it causes electrostatic repulsion forces with methylene

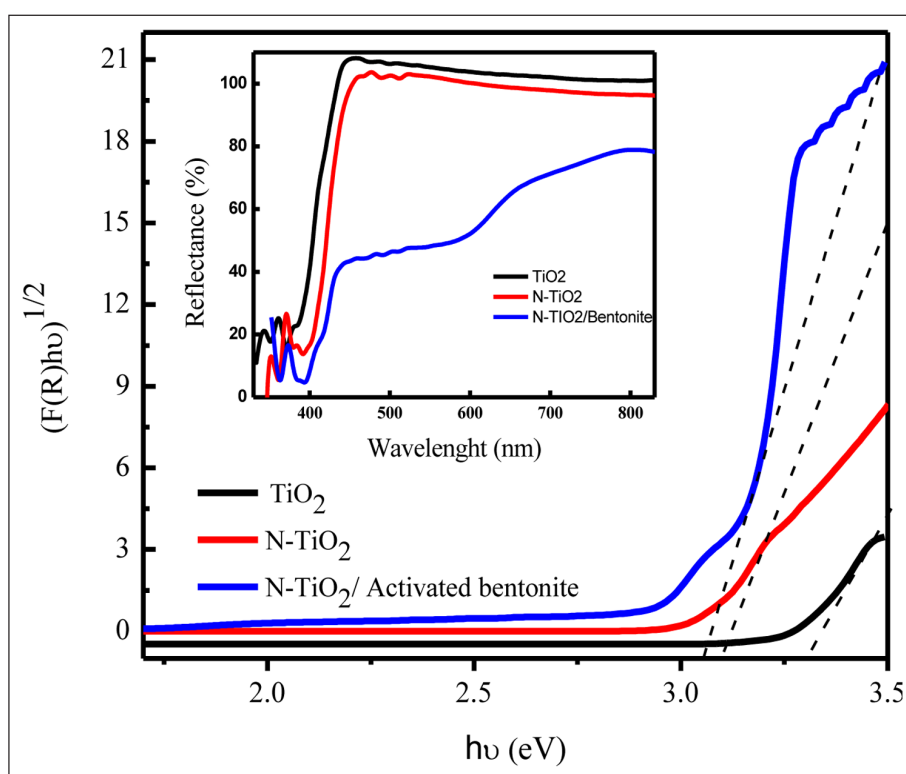
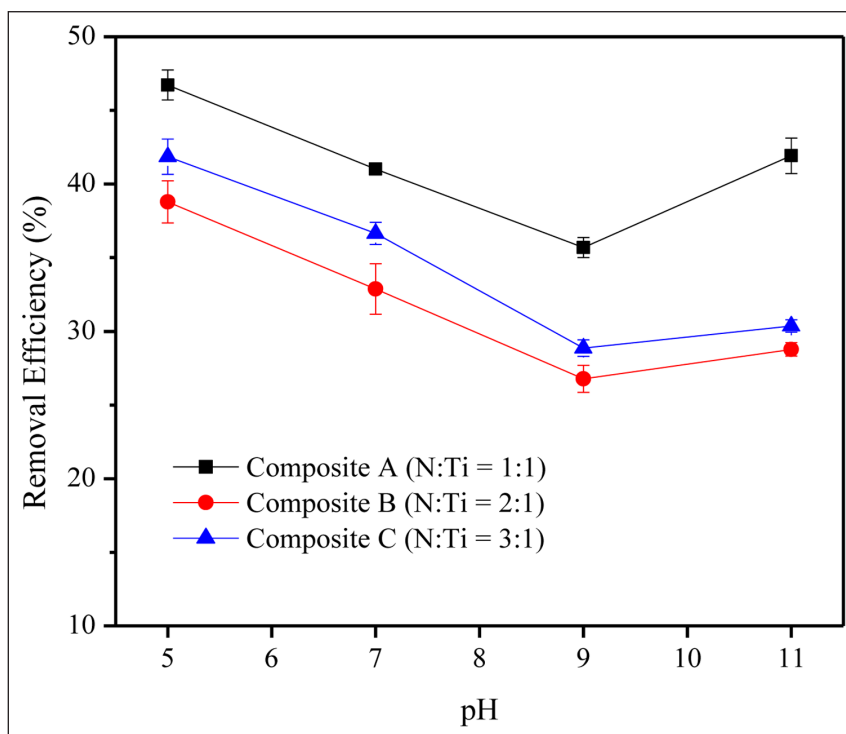


Figure 5 Tauc Plot of TiO<sub>2</sub>, N-TiO<sub>2</sub> (N:Ti = 1:1) and N-TiO<sub>2</sub>/Activated Bentonite (with N:Ti = 1:1).

SAMPLE	WAVELENGTH (nm)	ENERGY (eV)
TiO <sub>2</sub>	380	3.26
N-TiO <sub>2</sub> (with N:Ti = 1:1)	395	3.14
N-TiO <sub>2</sub> /Activated Bentonite (with N:Ti = 1:1)	405	3.06

**Table 3** Wavelength and Bandgap Energy.



**Figure 6** Effect of pH on The Removal Efficiency of Methylene Blue.

blue molecules, thereby reducing the adsorption ability of methylene blue. In addition, at high pH, the removal of methylene blue tends to be lower due to the formed hydroxyl radicals, which are quickly scavenged, thereby reducing the ability to react with the dye (Alkaim et al., 2014).

### 3.3. EFFECT OF IRRADIATION TIME ON METHYLENE BLUE REMOVAL

Figure 7 shows methylene blue's removal ability increased with increasing irradiation time. The maximum removal of methylene blue using activated N-TiO<sub>2</sub>/activated bentonite occurred at 120 minutes of irradiation. Tests using the ratio of N: Ti (1:1; 2:1 and 3:1) with a UV lamp photon source obtained the effectiveness of methylene blue removal of 99.23%, 98.93%, and 97.35%, respectively. Irradiation with visible lamp conditions with a ratio of N: Ti (1:1; 2:1 and 3:1) obtained removal effectiveness of 87.20%, 81.40%, and 77.74blitar%, respectively. The effect of irradiation time on the removal efficiency of methylene blue can be seen in Figure 8. This study's results indicate that N doping on TiO<sub>2</sub> removes methylene blue in UV and visible light irradiation, demonstrating how using N doping on TiO<sub>2</sub> materials and UV and visible light irradiation could

speed up the breakdown of methylene blue. Dopants were used to increase the amount of electron-hole pairs and the likelihood that the reaction would result in reactive species in hydroxide radicals by acting as a trap for electrons produced during the photogeneration process (Leong et al., 2022). Table 4 compares the performance of the N-TiO<sub>2</sub>/bentonite composite catalyst with other TiO<sub>2</sub>-based composite catalysts in removing methylene blue. The results of this study indicate that the composite catalyst N-TiO<sub>2</sub>/bentonite under UV and visible light irradiation conditions has higher removal efficiencies on lower dosages (2.5–10 times lower in dosage), higher initial methylene blue concentration (1.25–2.5 times higher in concentration), and shorter reaction (1.5–3 times shorter in irradiation time) than composite catalysts from previous studies' results.

The efficacy of eliminating methylene blue under either the off state or irradiation was inversely proportional to the rise in the N: Ti ratio. Irie et al. (2003) claim TiO<sub>2</sub> could develop many oxygen vacancies due to high nitrogen doping. Photoexcited electrons and positive holes recombine in the presence of TiO<sub>2</sub> crystal defects, which affects the photocatalytic activity. Increasing the dopant concentration can slow down photodegradation which

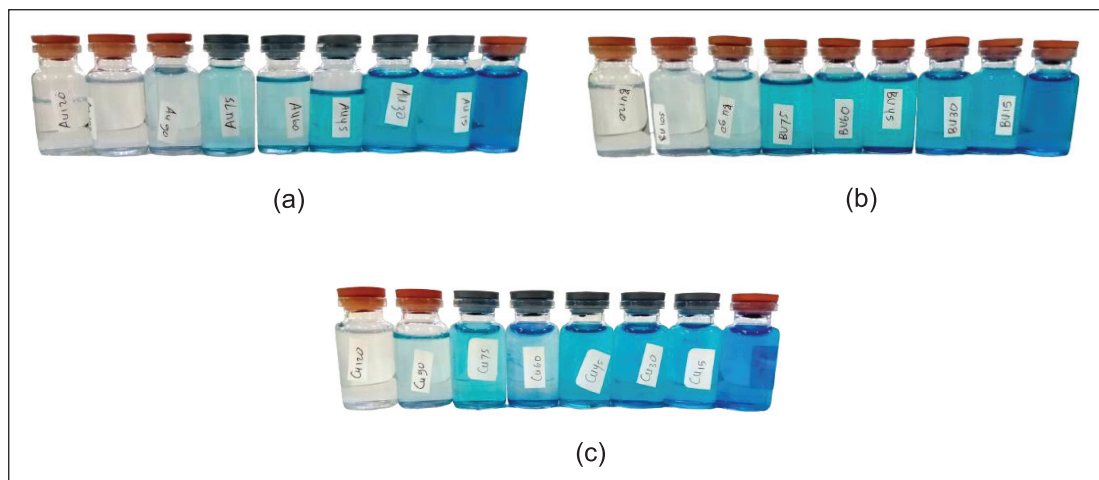


**Figure 7** Photocatalytic Process Results using **a.)** Composite A (N:Ti = 1:1); **b)** Composite B (N:Ti = 2:1); Composite C (N:Ti = 3:1).

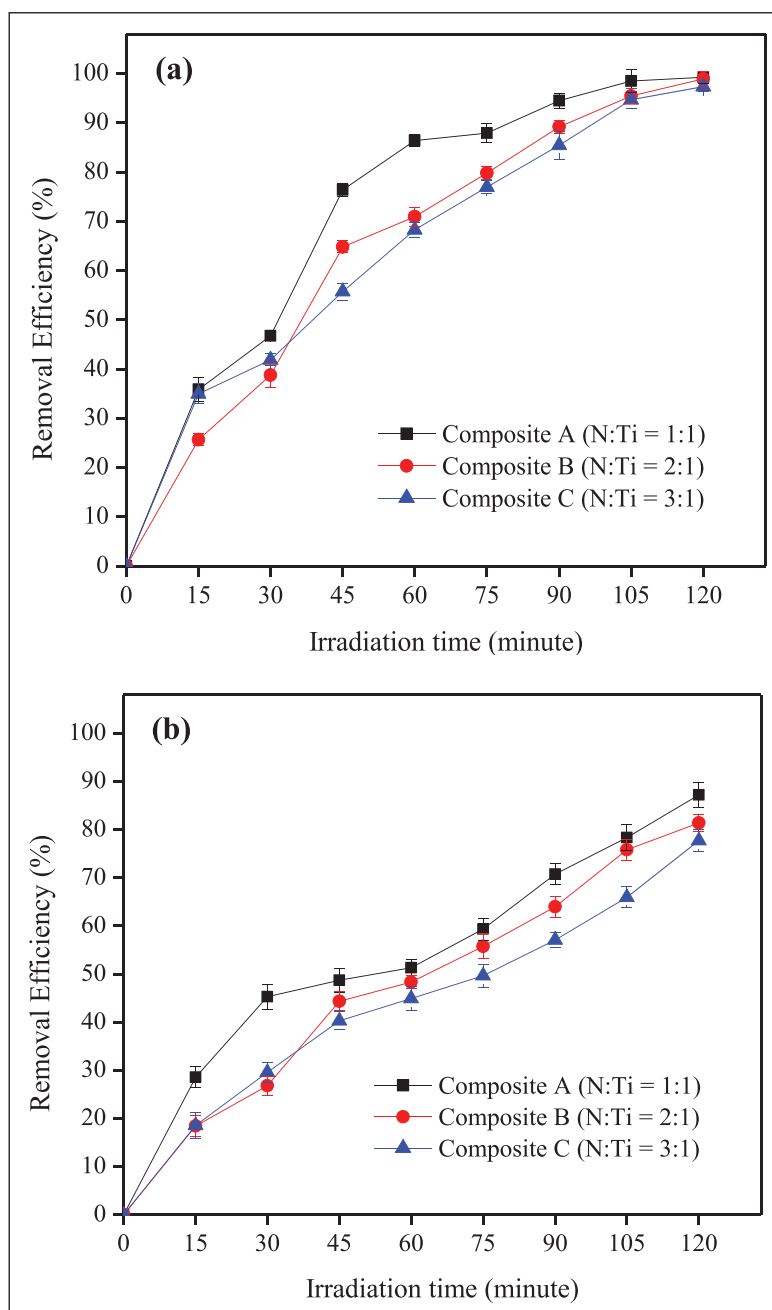


**Figure 8** Effect of Irradiation Time on The Removal Efficiency of Methylene Blue using **a.)** UV Lamp; **b.)** Visible Light Lamp.

MATERIALS	MB CONCENTRATION	SOLUTION PH	CATALYST DOSE	IRRADIATION	IRRADIATION TIME	REMOVAL	REFERENCE
Cu-doped TiO <sub>2</sub> films 10 mg/L		7	26.31 mg/L	Visible light (430 nm)	4 hr (batch)	95%	(Yang et al., 2018)
TCP/P/CuPOM/TiO <sub>2</sub> film	10 mg/L	–	100 mg/L	Visible light	5 hr (batch)	49%	(Sanguino et al., 2022)
TiO <sub>2</sub> treated NaOH	10 mg/L	–	200 mg/L	UV light (Xe lamp)	2.5 hr (batch)	90%	(Hou et al., 2018)
TiO <sub>2</sub> - montmorillonite	32 mg/L	6.5	160 mg/L	UV A light (365 nm)	6 hr (batch)	93.2%	(Djellabi et al., 2015)
40% TiO <sub>2</sub> -doped Calcined Mussel Shells	10 mg/L	6.3	2000 mg/L	UV A light (300–450 nm)	4 hr (batch)	95%	(Echabbi et al., 2019)
TiO <sub>2</sub> doped CuFe <sub>2</sub> O <sub>4</sub>	20 mg/L	–	500 mg/L	Visible light (Xe lamp)	3 hr (batch)	83.7%	(Arifin et al., 2019)
N-TiO <sub>2</sub> /bentonite (N:Ti = 1:1)	25 mg/L	5	200 mg/L	UV light* & Visible light**	2 hr (batch)	99.23* 87.20**	This study

**Table 4** Comparison with the previous research.

might be because many N atoms step in to replace O atoms, creating oxygen and Ti<sup>3+</sup> vacancies. Ti<sup>3+</sup> and many oxygen vacancies turn into photoinduction centers for hole recombination and electrons (h<sup>+</sup>/e<sup>-</sup>), which lowers the photocatalytic activity (Mahendrasingh et al., 2020).

### 3.4. PHOTOCATALYST REACTION KINETICS

A reaction kinetics analysis was performed to ascertain the mechanism of methylene blue reduction by activated N-TiO<sub>2</sub>/activated bentonite and the reduction rate at a specific time. Figure 9 shows the kinetic curve for methylene blue degradation by N-TiO<sub>2</sub>/activated bentonite. Based on the regression value (R<sup>2</sup>) of the pseudo-first-order, the kinetic trend of the methylene blue reaction is near 1. Table 5 shows the findings of examining the kinetic parameters for the methylene blue degradation by N-TiO<sub>2</sub>/activated bentonite.

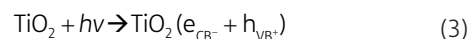
According to the findings of the kinetic analysis, lowering the N: Ti ratio led to a reduction in the reaction rate constant. When the N: Ti ratio is 1:1, the value of k reaches its highest value with a value of 0.0423 min<sup>-1</sup>. These parameter values have been confirmed based on the efficiency of methylene blue deterioration under the influence of UV light. Comparing the conditions of the ratios of 2:1 and 3:1, the ratio of 1:1 N: Ti tends to cause a quicker rate of methylene blue degradation. The photocatalytic activity diminishes as the N: Ti ratio rises because less TiO<sub>2</sub> is present in the photocatalyst material. Due to the abundance of N atoms that replace O, oxygen and Ti<sup>3+</sup> vacancies create photoinduction holes and electrons, which decreases photocatalytic activity.

### 3.5. METHYLENE BLUE PHOTODEGRADATION MECHANISM

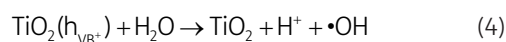
The attachment of pollutants to the surface of activated bentonite, which is later destroyed by hydroxyl ions, is

the basis of the photocatalysis-adsorption method's operation. The stimulation of the semiconductor material by photons from the light source, which causes the production of hydroxyl radicals, causes the degradation process to occur (Agrios & Pichat, 2005). In order to create holes (h<sup>+</sup> holes), electrons in the valence band must be excited to move into the conduction band. While electrons (e<sup>-</sup>) react with oxygen to make superoxide, which then reacts with water to produce radicals with the formula •OH, the hole first reacts with water to produce these radicals. The hydroxyl radicals will interact with the dyes to create environmentally safe derivative chemicals.

Radiation causes photoelectrons to be stimulated from the valence band to the conduction band, which leads to photocatalyst processes. The energy of the absorbed photon is equivalent to or higher than the semiconductor photocatalyst's band gap energy. An electron pair (e<sup>-</sup>) and a hole (h<sup>+</sup>) are produced as a result of the excitation process, as shown in Reaction Equation (3) (Ajmal et al., 2014).



Following a water ionization reaction, the photogenerated holes in the valence band produce •OH. Due to the irradiation of the semiconductor surface, the OH radical is a highly potent oxidizing agent. The Reaction Equations (4) and (5) (Ajmal et al., 2014) show how the ionization of water occurs.



When oxygen and electrons in the conduction band (e<sub>CB</sub><sup>-</sup>) interact, anionic superoxide radicals are created,

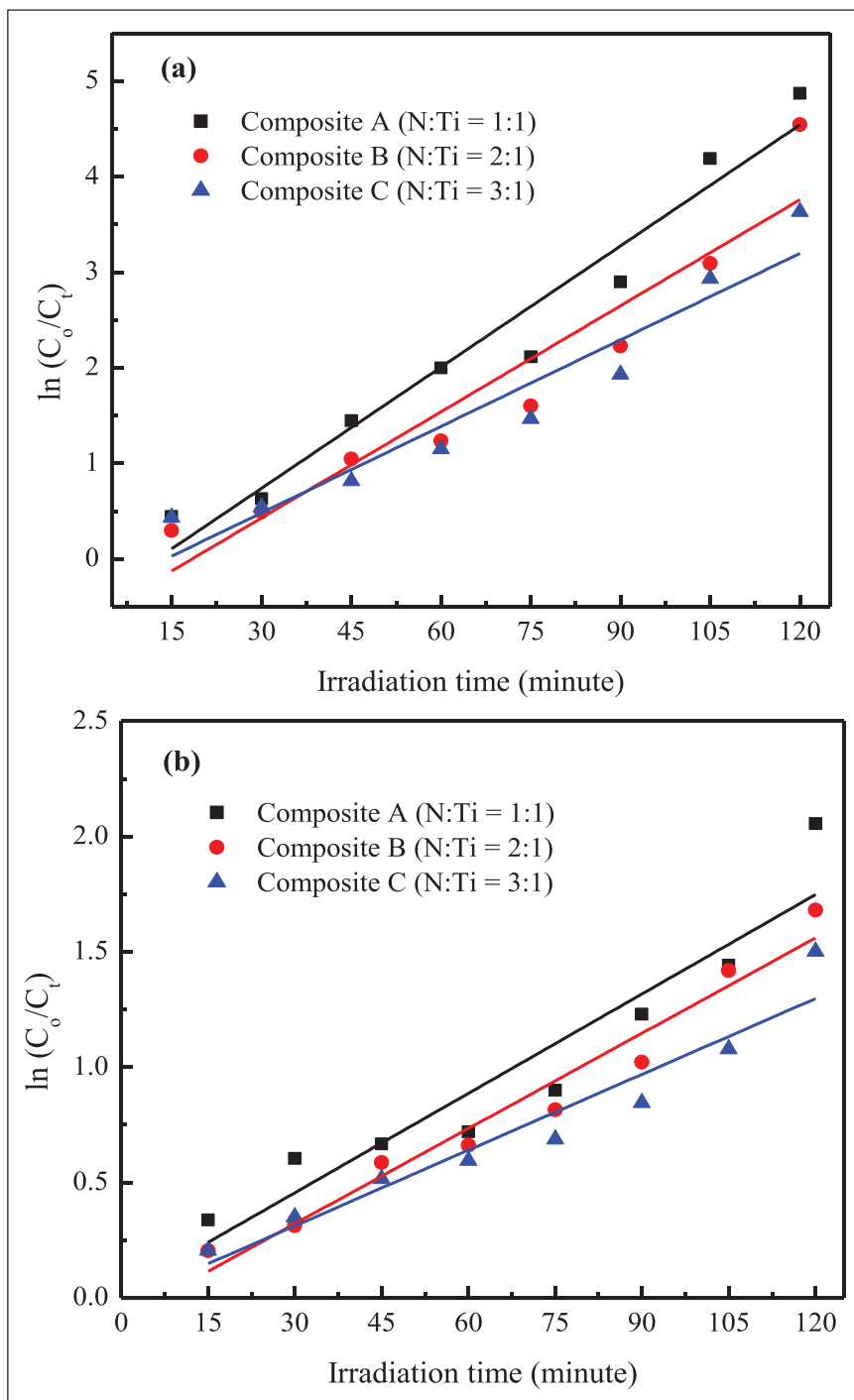
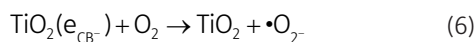


**Figure 9** Kinetic plot for photocatalytic degradation of methylene blue by irradiation (a) UV light (b) visible light Lamp.

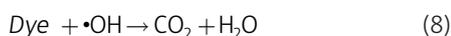
KINETIC MODEL	COMPOSITE		
	A (N:Ti = 1:1)	B (N:Ti = 2:1)	C (N:Ti = 3:1)
Langmuir-Hinshelwood (UV light)			
$k_{app}$ (minute <sup>-1</sup> )	0.0423	0.037	0.0302
R <sup>2</sup>	0.952	0.907	0,923
Langmuir-Hinshelwood (Visible light)			
$k_{app}$ (minute <sup>-1</sup> )	0,0144	0.0138	0.0110
R <sup>2</sup>	0.903	0.964	0.932

**Table 5** Kinetics Analysis of Photocatalytic Process Reaction.

leading to oxygen ions' absorption ( $O_2^-$ ). In addition to its function in oxidation, the generation of superoxide ions. The reaction equation shows how oxygen ions are absorbed (6) and (7) (Ajmal et al., 2014).



Superoxide is protonated by  $O_2$ , creating hydroperoxyl radicals ( $HO_2$ ) that break down into highly reactive hydroxyl radicals and react with methylene blue to create environmentally safe degradation products as explained in the reaction equation (8) (Giannakoudakis et al., 2022).



## 4. CONCLUSION

The composite catalyst had been successfully produced through a simple method consisting of a sonication process followed by calcination. The photocatalyst activity of N-TiO<sub>2</sub>/activated bentonite effectively reduces the concentration of methylene blue in wastewater. The maximum efficiency of methylene blue removal occurs when the ratio of N to Ti is 1:1, with 120 minutes of radiation of 99.23% and 87.20% under ultraviolet and visible light, respectively. The optimum pH condition for the photocatalyst process in removing methylene blue occurs at pH 5. The best nitrogen doping is at a ratio of N: Ti (1:1) with a bandgap energy of N-TiO<sub>2</sub>/bentonite of 3.06 eV at a wavelength of 338 nm. Increasing irradiation time tends to cause an increase in methylene blue removal activity in the photocatalyst process. The N-TiO<sub>2</sub>/bentonite composite catalyst is effective in the UV and visible light photocatalytic process. N-TiO<sub>2</sub>/bentonite photocatalysts can be used as an alternative option that is cheap and environmentally friendly for application on an industrial scale, especially for treating wastewater containing methylene blue.

## FUNDING INFORMATION

This research was financially supported by the Center for Research and Community Service Shipbuilding Institute of Polytechnic Surabaya.

## COMPETING INTERESTS

The authors have no competing interests to declare.

## AUTHOR CONTRIBUTIONS

**Adhi Setiawan:** Conceptualization, method investigation, data investigation, supervision, writing, editing, review. **Vira Fadilah Qur'ani:** Method investigation, data investigation. **Tarikh Azis Ramadani:** Method investigation, data investigation, supervision. **Mochamad Luqman Ashari:** Writing, review. **Denny Dermawan:** Conceptualization, supervision, writing, editing, review. **Aditya Prana Iswara:** Conceptualization, supervision, writing, review.

## AUTHOR AFFILIATIONS

**Adhi Setiawan**  [orcid.org/0000-0001-5959-7970](https://orcid.org/0000-0001-5959-7970)

Waste Treatment Engineering Study Program, Shipbuilding Institute of Polytechnic Surabaya, Jalan Teknik Kimia, Kampus ITS Sukolilo, Surabaya, Indonesia; Waste Treatment Laboratory, Shipbuilding Institute of Polytechnic Surabaya, Jalan Teknik Kimia, Kampus ITS Sukolilo, Surabaya, Indonesia

**Vira Fadilah Qur'ani**

Waste Treatment Engineering Study Program, Shipbuilding Institute of Polytechnic Surabaya, Jalan Teknik Kimia, Kampus ITS Sukolilo, Surabaya, Indonesia

**Tarikh Azis Ramadani**  [orcid.org/0009-0006-9289-1884](https://orcid.org/0009-0006-9289-1884)

Waste Treatment Engineering Study Program, Shipbuilding Institute of Polytechnic Surabaya, Jalan Teknik Kimia, Kampus ITS Sukolilo, Surabaya, Indonesia; Waste Treatment Laboratory, Shipbuilding Institute of Polytechnic Surabaya, Jalan Teknik Kimia, Kampus ITS Sukolilo, Surabaya, Indonesia

**Mochamad Luqman Ashari**

Safety Engineering Study Program, Shipbuilding Institute of Polytechnic Surabaya, Jalan Teknik Kimia, Kampus ITS Sukolilo, Surabaya, Indonesia

**Denny Dermawan**  [orcid.org/0000-0001-5805-3322](https://orcid.org/0000-0001-5805-3322)

Waste Treatment Engineering Study Program, Shipbuilding Institute of Polytechnic Surabaya, Jalan Teknik Kimia, Kampus ITS Sukolilo, Surabaya, Indonesia; Waste Treatment Laboratory, Shipbuilding Institute of Polytechnic Surabaya, Jalan Teknik Kimia, Kampus ITS Sukolilo, Surabaya, Indonesia

**Aditya Prana Iswara**  [orcid.org/0000-0001-5178-1298](https://orcid.org/0000-0001-5178-1298)

Department of Disaster Management, Postgraduate School, Universitas Airlangga, Surabaya, Indonesia

## REFERENCES

- Agrios, AG and Pichat, P.** 2005. State of the art and perspectives on materials and applications of photocatalysis over TiO<sub>2</sub>. *Journal of Applied Electrochemistry*, 35(7-8): 655-663. DOI: <https://doi.org/10.1007/s10800-005-1627-6>
- Ajmal, A, Majeed, I, Malik, RN, Idriss, H and Nadeem, MA.** 2014. Principles and mechanisms of photocatalytic dye degradation on TiO<sub>2</sub> based photocatalysts: A comparative

- overview. *RSC Advances*, 4(70): 37003–37026. DOI: <https://doi.org/10.1039/c4ra06658h>
- Alkaim, AF, Aljeboree, AM, Alrazaq, NA, Baqir, SJ, Hussein, FH, Lilo, AJ.** 2014. Effect of pH on Adsorption and Photocatalytic Degradation Efficiency of Different Catalysts on Removal of Methylene Blue. *Asian Journal of Chemistry*, 26: 8445–8448. DOI: <https://doi.org/10.14233/ajchem.2014.17908>
- Ansari, SA, Khan, MM, Ansari, MO and Cho, MH.** 2016. Nitrogen-doped titanium dioxide (N-doped TiO<sub>2</sub>) for visible light photocatalysis. *New Journal of Chemistry*, 40(4): 3000–3009. DOI: <https://doi.org/10.1039/c5nj03478g>
- Anwer, H and Park, JW.** 2019. Near-infrared to visible photon transition by upconverting NaYF<sub>4</sub>: Yb<sup>3+</sup>, Gd<sup>3+</sup>, Tm<sup>3+</sup>@Bi<sub>2</sub>WO<sub>6</sub> core@shell composite for bisphenol A degradation in solar light. *Applied Catalysis B: Environmental*, 243: 438–447. DOI: <https://doi.org/10.1016/j.apcatb.2018.10.074>
- Arifin, MN, Rezaul Karim, KM, Abdullah, H and Khan, MR.** 2019. Synthesis of titania doped copper ferrite photocatalyst and its photoactivity towards methylene blue degradation under visible light irradiation. *Bulletin of Chemical Reaction Engineering & Catalysis*, 14(1): 219–227. DOI: <https://doi.org/10.9767/bcrec.14.1.3616.219-227>
- Bakre, PV, Tilve, SG and Shirsat, RN.** 2020. Influence of N sources on the photocatalytic activity of N-doped TiO<sub>2</sub>. *Arabian Journal of Chemistry*, 13(11): 7637–7651. DOI: <https://doi.org/10.1016/j.arabjc.2020.09.001>
- Benhouria, A, Islam, MA, Zaghouane-Boudiaf, H, Boutahala, M and Hameed, BH.** 2015. Calcium alginate-bentonite-activated carbon composite beads as highly effective adsorbent for methylene blue. *Chemical Engineering Journal*, 270: 621–630. DOI: <https://doi.org/10.1016/j.cej.2015.02.030>
- Calisir, MD, Gungor, M, Demir, A, Kilic, A and Khan, MM.** 2020. Nitrogen-doped TiO<sub>2</sub> fibers for visible-light-induced photocatalytic activities. *Ceramics International*, 46(10): 16743–16753. DOI: <https://doi.org/10.1016/j.ceramint.2020.03.250>
- Chang, YS, Au, PI, Mubarak, NM, Khalid, M, Jagadish, P, Walvekar, R and Abdullah, EC.** 2020. Adsorption of Cu(II) and Ni(II) ions from wastewater onto bentonite and bentonite/GO composite. *Environmental Science and Pollution Research*, 27(26): 33270–33296. DOI: <https://doi.org/10.1007/s11356-020-09423-7>
- Chen, D, Du, G, Zhu, Q and Zhou, F.** 2013. Synthesis and characterization of TiO<sub>2</sub> pillared montmorillonites: Application for methylene blue degradation. *Journal of Colloid and Interface Science*, 409: 151–157. DOI: <https://doi.org/10.1016/j.jcis.2013.07.049>
- Chien, C-L, Iswara, AP, Liou, Y-L, Wang, B-T, Chang, J-C, Hung, Y-H and Tsai, C-J.** 2015. A real-time monitoring system for soluble gas pollutants and its application for determining the control efficiency of packed towers. *Separation and Purification Technology*, 154: 137–148. DOI: <https://doi.org/10.1016/j.seppur.2015.09.033>
- Daghrir, R, Drogui, P and Robert, D.** 2013. Modified TiO<sub>2</sub> for environmental photocatalytic applications: A review. *Industrial and Engineering Chemistry Research*, 52(10): 3581–3599. DOI: <https://doi.org/10.1021/ie303468t>
- Dermawan, D, Nur, A, Eka, E, Setyawati, P, Pham, M, Jiang, J, You, S and Wang, Y.** 2022. *Industrial Crops & Products* The potential of transforming rice straw (*Oryza sativa*) and golden shower (*Cassia fistula*) seed waste into high-efficiency biochar by atmospheric pressure microwave plasma, 185(May). DOI: <https://doi.org/10.1016/j.indcrop.2022.115122>
- Dilaver, M, Hocaoglu, SM, Soydemir, G, Dursun, M, Keskinler, B, Koyuncu, İ and Ađtas, M.** 2018. Hot wastewater recovery by using ceramic membrane ultrafiltration and its reusability in the textile industry. *Journal of Cleaner Production*, 171: 220–233. DOI: <https://doi.org/10.1016/j.jclepro.2017.10.015>
- Djellabi, R, Ghorab, MF, Cerrato, G, Morandi, S, Gatto, S, Oldani, V, Di Michele, A and Bianchi, CL.** 2015. Photoactive TiO<sub>2</sub>-montmorillonite composite for degradation of organic dyes in water. *Journal of Photochemistry and Photobiology A: Chemistry*, 295: 57–63. DOI: <https://doi.org/10.1016/j.jphotochem.2014.08.017>
- Echabbi, F, Hamlich, M, Harkati, S, Jouali, A, Tahiri, S, Lazar, S, Lakhmiri, R and Safi, M.** 2019. Photocatalytic degradation of methylene blue by the use of titanium-doped Calcined Mussel Shells CMS/TiO<sub>2</sub>. *Journal of Environmental Chemical Engineering*, 7(5): 103293. DOI: <https://doi.org/10.1016/j.jece.2019.103293>
- Fayoud, N, Tahiri, S, Alami Younsi, S, Albizane, A, Gallart-Mateu, D, Cervera, ML and de la Guardia, M.** 2016. Kinetic, isotherm and thermodynamic studies of the adsorption of methylene blue dye onto agro-based cellulosic materials. *Desalination and Water Treatment*, 57(35): 16611–16625. DOI: <https://doi.org/10.1080/19443994.2015.1079249>
- Gar Alalm, M, Tawfik, A and Ookawara, S.** 2016. Solar photocatalytic degradation of phenol by TiO<sub>2</sub>/AC prepared by temperature impregnation method. *Desalination and Water Treatment*, 57(2): 835–844. DOI: <https://doi.org/10.1080/19443994.2014.969319>
- Giannakoudakis, DA, Zormpa, FF, Margellou, AG, Qayyum, A, Colmenares-Quintero, RF, Len, C, Colmenares, JC and Triantafyllidis, KS.** 2022. Carbon-Based Nanocatalysts (CnCs) for Biomass Valorization and Hazardous Organics Remediation. *Nanomaterials*, 12(10). DOI: <https://doi.org/10.3390/nano12101679>
- Gil, A, García, AM, Fernández, M, Vicente, MA, González-Rodríguez, B, Rives, V and Korili, SA.** 2017. Effect of dopants on the structure of titanium oxide used as a photocatalyst for the removal of emergent contaminants. *Journal of Industrial and Engineering Chemistry*, 53: 183–191. DOI: <https://doi.org/10.1016/j.jiec.2017.04.024>
- Gong, X, Wang, H, Yang, C, Li, Q, Chen, X and Hu, J.** 2015. Photocatalytic degradation of high ammonia concentration wastewater by TiO<sub>2</sub>. *Future Cities and*

- Environment*, 1: 12. DOI: <https://doi.org/10.1186/s40984-015-0012-9>
- Hadj Bachir, D, Khalaf, H, Ferroukhi, S, Boutoumi, Y, Schnee, J and Gaigneaux, EM.** 2020. Preparation and characterization of TiO<sub>2</sub> pillared clay: Effect of palladium and photosensitizer on photocatalytic activity. *Research Journal of Chemistry and Environment*, 24(3): 60–73.
- Hoang, S, Guo, S and Mullins, CB.** 2012. Coincorporation of N and Ta into TiO<sub>2</sub> nanowires for visible light-driven photoelectrochemical water oxidation. *Journal of Physical Chemistry C*, 116(44): 23283–23290. DOI: <https://doi.org/10.1021/jp309743u>
- Hou, C, Hu, B and Zhu, J.** 2018. Photocatalytic degradation of methylene blue over TiO<sub>2</sub> pretreated with varying concentrations of NaOH. *Catalysts*, 8(12). DOI: <https://doi.org/10.3390/catal8120575>
- Hrachová, J, Madejová, J, Billik, P, Komadel, P and Fajnor, VŠ.** 2007. Dry grinding of Ca and octadecyltrimethylammonium montmorillonite. *Journal of Colloid and Interface Science*, 316(2): 589–595. DOI: <https://doi.org/10.1016/j.jcis.2007.07.085>
- Huang, Z, Li, Y, Chen, W, Shi, J, Zhang, N, Wang, X, Li, Z, Gao, L and Zhang, Y.** 2017. Modified bentonite adsorption of organic pollutants of dye wastewater. *Materials Chemistry and Physics*, 202: 266–276. DOI: <https://doi.org/10.1016/j.matchemphys.2017.09.028>
- Imron, MF, Kurniawan, SB, Soegianto, A and Wahyudianto, FE.** 2019. Phytoremediation of methylene blue using duckweed (*Lemna minor*). *Heliyon*, 5(8): e02206. DOI: <https://doi.org/10.1016/j.heliyon.2019.e02206>
- Javanbakht, V and Mohammadian, M.** 2021. Photo-assisted advanced oxidation processes for efficient removal of anionic and cationic dyes using Bentonite/TiO<sub>2</sub> nanoparticle immobilized with silver nanoparticles. *Journal of Molecular Structure*, 1239: 130496. DOI: <https://doi.org/10.1016/j.molstruc.2021.130496>
- Jawad, AH, Mubarak, NSA, Ishak, MAM, Ismail, K and Nawawi, WI.** 2016. Kinetics of photocatalytic decolorization of cationic dye using porous TiO<sub>2</sub> film. *Journal of Taibah University for Science*, 10(3): 352–362. DOI: <https://doi.org/10.1016/j.jtusci.2015.03.007>
- Konstantinou, IK and Albanis, TA.** 2004. TiO<sub>2</sub>-assisted photocatalytic degradation of azo dyes in aqueous solution: Kinetic and mechanistic investigations: A review. *Applied Catalysis B: Environmental*, 49(1): 1–14. DOI: <https://doi.org/10.1016/j.apcatb.2003.11.010>
- Koswojo, R, Utomo, RP, Ju, YH, Ayucitra, A, Soetaredjo, FE, Sunarso, J and Ismadji, S.** 2010. Acid Green 25 removal from wastewater by organo-bentonite from Pacitan. *Applied Clay Science*, 48(1–2): 81–86. DOI: <https://doi.org/10.1016/j.clay.2009.11.023>
- Kuo, YL, Su, TL, Kung, FC and Wu, TJ.** 2011. A study of parameter setting and characterization of visible-light-driven nitrogen-modified commercial TiO<sub>2</sub> photocatalysts. *Journal of Hazardous Materials*, 190(1–3): 938–944. DOI: <https://doi.org/10.1016/j.jhazmat.2011.04.031>
- Leong, CY, Teh, HL, Chen, MC and Lee, SL.** 2022. Effect of Synthesis Methods on Properties of Copper Oxide Doped Titanium Dioxide Photocatalyst in Dye Photodegradation of Rhodamine B. *Science and Technology Indonesia*, 7(1): 91–97. DOI: <https://doi.org/10.26554/sti.2022.7.1.91-97>
- Li, J, Chen, C, Zhao, J, Zhu, H and Orthman, J.** 2002. Photodegradation of dye pollutants on TiO<sub>2</sub> nanoparticles dispersed in silicate under UV – VIS irradiation. *Applied Catalysis B: Environmental*, 37(4): 331–338. DOI: [https://doi.org/10.1016/S0926-3373\(02\)00011-5](https://doi.org/10.1016/S0926-3373(02)00011-5)
- Ma, X, Hao, K, Dai, Y, Song, L, Yu, Q, Yin, X and Wang, Z.** 2021. Enhanced Visible-Light Photocatalytic Activity by the Comprehensive Effects of Mesoporous and N-Doping at the Meso-N-TiO<sub>2</sub> Nanocatalysts. *ChemistrySelect*, 6(24): 6029–6036. DOI: <https://doi.org/10.1002/slct.202101243>
- Mahendrasingh, P, Vrushali, N, Manisha, G, Anita, K and Rahul, T.** 2020. Effect of Nitrogen Doping on Photocatalytic Activity of TiO<sub>2</sub>. *Journal of Nanoscience and Technology*, 6(4): 918–923. DOI: <https://doi.org/10.30799/jnst.312.20060401>
- Marques, J, Gomes, TD, Forte, MA, Silva, RF and Tavares, CJ.** 2019. A new route for the synthesis of highly-active N-doped TiO<sub>2</sub> nanoparticles for visible light photocatalysis using urea as nitrogen precursor. *Catalysis Today*, 326(July 2018): 36–45. DOI: <https://doi.org/10.1016/j.cattod.2018.09.002>
- Martins, AC, Cazetta, AL, Pezoti, O, Souza, JRB, Zhang, T, Pilau, EJ, Asefa, T and Almeida, VC.** 2017. Sol-gel synthesis of new TiO<sub>2</sub>/activated carbon photocatalyst and its application for degradation of tetracycline. *Ceramics International*, 43(5): 4411–4418. DOI: <https://doi.org/10.1016/j.ceramint.2016.12.088>
- Matos, J, Laine, J and Herrmann, JM.** 1998. Synergy effect in the photocatalytic degradation of phenol on a suspended mixture of titania and activated carbon. *Applied Catalysis B: Environmental*, 18(3–4): 281–291. DOI: [https://doi.org/10.1016/S0926-3373\(98\)00051-4](https://doi.org/10.1016/S0926-3373(98)00051-4)
- Natsir, M, Putri, YI, Wibowo, D, Maulidiyah, M, Salim, L, OA, Azis, T, Bijang, CM, Mustapa, F, Irwan, I, Arham, Z and Nurdin, M.** 2021. Effects of Ni-TiO<sub>2</sub> Pillared Clay–Montmorillonite Composites for Photocatalytic Enhancement Against Reactive Orange Under Visible Light. *Journal of Inorganic and Organometallic Polymers and Materials*, 31(8): 3378–3388. DOI: <https://doi.org/10.1007/s10904-021-01980-9>
- Pan, Y, Wang, Y, Zhou, A, Wang, A, Wu, Z, Lv, L, Li, X, Zhang, K and Zhu, T.** 2017. Removal of azo dye in an up-flow membrane-less bioelectrochemical system integrated with bio-contact oxidation reactor. *Chemical Engineering Journal*, 326: 454–461. DOI: <https://doi.org/10.1016/j.cej.2017.05.146>
- Rahardjo, AK, Susanto, MJJ, Kurniawan, A, Indraswati, N and Ismadji, S.** 2011. Modified Ponorogo bentonite for the removal of ampicillin from wastewater. *Journal of Hazardous Materials*, 190(1–3): 1001–1008. DOI: <https://doi.org/10.1016/j.jhazmat.2011.04.052>

- Ravi and Pandey, LM.** 2019. Enhanced adsorption capacity of designed bentonite and alginate beads for the effective removal of methylene blue. *Applied Clay Science*, 169(October 2018): 102–111. DOI: <https://doi.org/10.1016/j.clay.2018.12.019>
- Raza, N, Raza, W, Gul, H, Azam, M, Lee, J, Vikrant, K and Kim, KH.** 2020. Solar-light-active silver phosphate/titanium dioxide/silica heterostructures for photocatalytic removal of organic dye. *Journal of Cleaner Production*, 254: 120031. DOI: <https://doi.org/10.1016/j.jclepro.2020.120031>
- Rossetto, E, Petkowicz, DI, dos Santos, JHZ, Pergher, SBC and Penha, FG.** 2010. Bentonites impregnated with TiO<sub>2</sub> for photodegradation of methylene blue. *Applied Clay Science*, 48(4): 602–606. DOI: <https://doi.org/10.1016/j.clay.2010.03.010>
- Sanchez, M, Rivero, MJ and Ortiz, I.** 2010. Photocatalytic oxidation of grey water over titanium dioxide suspensions. *Desalination*, 262(1–3): 141–146. DOI: <https://doi.org/10.1016/j.desal.2010.05.060>
- Sanguino, A, Diaz-Urbe, C, Duran, F, Vallejo, W, Guzman, L, Ruiz, D, Puello, E, Quiñones, C, Schott, E and Zarate, X.** 2022. Photocatalytic Degradation of Methylene Blue under Visible Light Using TiO<sub>2</sub> Thin Films Impregnated with Porphyrin and Anderson-Type Polyoxometalates (Cu and Zn). *Catalysts*, 12(10). DOI: <https://doi.org/10.3390/catal12101169>
- Sasikala, SP, Nibila, TA, Babitha, KB, Peer Mohamed, AA and Solaiappan, A.** 2019. Competitive photo-degradation performance of ZnO-modified bentonite clay in water containing both organic and inorganic contaminants. *Sustainable Environment Research*, 1(1): 1–12. DOI: <https://doi.org/10.1186/s42834-019-0001-z>
- Setiawan, A, Dianti, LR, Mayangsari, NE, Widiana, DR and Dermawan, D.** 2023. Removal of methylene blue using heterogeneous Fenton process with Fe-impregnated kepok banana (*Musa acuminata* L.) peel activated carbon as catalyst. *Inorganic Chemistry Communications*, 152(January): 110715. DOI: <https://doi.org/10.1016/j.inoche.2023.110715>
- Setiawan, A, Mahfud, RNM, Mayangsari, NE, Widiana, DR, Iswara, AP and Dermawan, D.** 2024. The potential of using sweet corn (*Zea mays Saccharata*) husk waste as a source for biodegradable plastics. *Industrial Crops & Products*, 208(February 2024): 117760. DOI: <https://doi.org/10.1016/j.indcrop.2023.117760>
- Sinhmahapatra, A, Jeon, JP and Yu, JS.** 2015. A new approach to prepare highly active and stable black titania for visible light-assisted hydrogen production. *Energy and Environmental Science*, 8(12): 3539–3544. DOI: <https://doi.org/10.1039/c5ee02443a>
- Tichapondwa, SM, Newman, JP and Kubheka, O.** 2020. Effect of TiO<sub>2</sub> phase on the photocatalytic degradation of methylene blue dye. *Physics and Chemistry of the Earth*, 118–119: 102900. DOI: <https://doi.org/10.1016/j.pce.2020.102900>
- Toor, M, Jin, B, Dai, S and Vimonses, V.** 2015. Activating natural bentonite as a cost-effective adsorbent for removal of Congo-red in wastewater. *Journal of Industrial and Engineering Chemistry*, 21: 653–661. DOI: <https://doi.org/10.1016/j.jiec.2014.03.033>
- Wang, F, Zhang, H, Du, M, Li, J, Yang, P, Yu, T, Wang, Y and Qu, C.** 2021. Effects of TiO<sub>2</sub>/Bentonite on the Pyrolysis Process of Oily Sludge. *Nature Environment and Pollution Technology*, 20(1): 1–12. DOI: <https://doi.org/10.46488/NEPT.2021.V20I01.001>
- Wang, W, Lin, F, Yan, B, Cheng, Z, Chen, G, Kuang, M, Yang, C and Hou, L.** 2020. The role of seashell wastes in TiO<sub>2</sub>/Seashell composites: Photocatalytic degradation of methylene blue dye under sunlight. *Environmental Research*, 188: 109831. DOI: <https://doi.org/10.1016/j.envres.2020.109831>
- Yang, CC, Doong, RA, Chen, KF, Chen, GS and Tsai, YP.** 2018. The photocatalytic degradation of methylene blue by green semiconductor films that is induced by irradiation by a light-emitting diode and visible light. *Journal of the Air and Waste Management Association*, 68(1): 29–38. DOI: <https://doi.org/10.1080/10962247.2017.1358222>
- Yeoh, ME and Chan, KY.** 2017. Recent advances in photo-anode for dye-sensitized solar cells: a review. *International Journal of Energy Research*, 41(15): 2446–2467. DOI: <https://doi.org/10.1002/er.3764>
- Zhang, J, Xu, LJ, Zhu, ZQ and Liu, QJ.** 2015. Synthesis and properties of (Yb, N)-TiO<sub>2</sub> photocatalyst for degradation of methylene blue (MB) under visible light irradiation. *Materials Research Bulletin*, 70: 358–364. DOI: <https://doi.org/10.1016/j.materresbull.2015.04.060>

---

**TO CITE THIS ARTICLE:**

Setiawan, A, Qur'ani, VF, Ramadani, TA, Ashari, ML, Dermawan, D and Iswara, AP. 2024. Potential of Local Natural Bentonite Impregnated with N-TiO<sub>2</sub> to Degrade Methylene Blue Using Photocatalytic Process. *Future Cities and Environment*, 10(1): 14, 1-17. DOI: <https://doi.org/10.5334/fce.220>

**Submitted:** 31 October 2023    **Accepted:** 12 June 2024    **Published:** 24 June 2024

**COPYRIGHT:**

© 2024 The Author(s). This is an open-access article distributed under the terms of the Creative Commons Attribution 4.0 International License (CC-BY 4.0), which permits unrestricted use, distribution, and reproduction in any medium, provided the original author and source are credited. See <http://creativecommons.org/licenses/by/4.0/>.

*Future Cities and Environment* is a peer-reviewed open access journal published by Ubiquity Press.

